ChemSusChem

Chemistry Europe
European Chemical Societies Publishing
ChemSusChem

RESEARCH ARTICLE OPEN ACCESS

Prospective Environmental Impact Assessment of Scaling Up Perovskite/Silicon Tandem Solar Cells to Industrial Applications

Mercy Jelagat Kipyator[1] | Federico Rossi[2] | Jaume-Adrià Alberola-Borràs[3] | Rosario Vidal[3] | Maria Laura Parisi[1,4,5] | Adalgisa Sinicropi[1,4,5]

[1]Department of Biotechnology, Chemistry and Pharmacy, R[2]ES Lab, University of Siena, Siena, Italy | [2]Interdisciplinary Centre for Sustainability and Climate, Sant'Anna School of Advanced Studies, Pisa, Italy | [3]Institute of Advanced Materials (INAM), Universitat Jaume I, Castelló de la Plana, Spain | [4]Centre for Colloid and Surface Science (CSGI), Sesto Fiorentino, Italy | [5]Institute of Chemistry of Organometallic Compounds (CNR-ICCOM), Sesto Fiorentino, Italy

Correspondence: Adalgisa Sinicropi (adalgisa.sinicropi@unisi.it)

Received: 24 October 2025 | **Revised:** 13 March 2026 | **Accepted:** 30 March 2026

Keywords: eco-design | perovskite/silicon | prospective LCA | sustainability | upscaling

ABSTRACT

Perovskite–silicon tandem solar cells (TSC) are considered a promising technology. However, their transitions from lab prototypes to industrial scale pose environmental concerns. This study presents a prospective life cycle assessment (LCA) of four potential designs of perovskite–silicon tandem cells (TSC 1, TSC 2, TSC 3, TSC 4). By modeling future-oriented scenarios, we analyze and present results for four LCA metrics: global warming potential (GWP), cumulative energy demand (CED), energy payback time (EPBT), and carbon payback time (CO_2PBT). Results show that the carbon footprint and energy consumption of tandem solar devices are expected to decrease over time, indicating that they will demonstrate better environmental performance compared to single-junction silicon devices. Among the tandem designs analyzed, TSC 3 exhibits the lowest environmental impact per m^2; however, TSC 4 shows superior environmental performance per kWh for all assessed impact categories. The analysis highlights that although material selection is crucial, optimizing the overall device architecture to enhance efficiency is equally important in achieving tandem devices with a low environmental footprint. Key recommendations for optimizing the tandem architecture include reducing the silicon wafer thickness in future tandem designs, the use of thinner indium-based transparent conductive oxide, and prioritizing recycling and re-use of the critical materials.

1 | Introduction

Solar energy is considered a cornerstone energy source in transitioning to a sustainable energy future [1]. One of the most common applications of solar energy is photovoltaic (PV) technology, which converts sunlight into electricity. In the last seven decades, researchers have developed various materials and architectures for PV technology, starting from first-generation (1G) solar cells, which include single-crystalline and monocrystalline silicon (Si), second-generation (2G) that include thin-film cells and modules (amorphous silicon, cadmium telluride, and copper indium gallium [2]), and the third generation (3G), which consists of emerging organic-based, inorganic, or hybrid solar cell technologies such as dye-sensitized solar cells (DSSCs), quantum dot solar cells, and perovskite solar cells (PSCs) [3].

With current PV panel installation accounting for ~10% of the world's electricity generation, there is a strong motivation for the development of very high-efficiency technologies [4] to drive down the cost of PV installation. One common approach to improving the overall power conversion efficiency (PCE) of solar cells is combining multiple single-junction solar cells (also called "subcells") in a tandem configuration [5]. In particular, the tandem architecture combining perovskites and silicon (PSC–Si) is considered one of the

most promising configurations due to the advantages offered by the perovskite such as high-efficiency potential, low production costs, tunable bandgap, and the advantages from combination with silicon technologies [6].

PSC–Si can be combined in three ways: two-terminal (2T), where the PSC will be in direct contact with the silicon cell through a series connection; four-terminal (4T), where the PSC and silicon will be electrically separated; and three-terminal (3T), where the top PSC and silicon subcells share a common terminal while maintaining their independent terminals [7]. Among these configurations, the 2T has more potential for industrial applications mainly because it offers a good balance between enhanced performance, low costs, and complexity of assembly. With the 4T requiring two sets of electrical contacts and the 3T requiring an additional terminal, they present extra cost and processing steps, making the 2T the most viable choice for initial industrialization of this technology [8]. The 2T tandem PSC–Si solar cells can be categorized as negative-intrinsic-positive (NIP) or positive-intrinsic-negative (PIN) 2T PSC–Si depending on the stacking order of the layers in the PSC subcell.

The current highest certified efficiency value for 2T PSC–Si tandem cell at laboratory scale is 35% [9, 10]. This value now exceeds the theoretical efficiency limit for any single-junction cell technology. With the potential for even higher efficiency and the possibility of further enhancements, they are now on the transition from research laboratories to the industry. Nevertheless, for solar cell technology to reach commercialization, it should satisfy certain technological, economic, and social factors that include having high efficiency, be scalable, be stable, cost-competitive, and environmentally friendly [11]. Hence, moving from laboratory scale to stable industrial PSC–Si tandem solar cells (TSCs) is a huge task that still requires scientific and technological advancements throughout PSC–Si TSC's entire commercialization timeline. This encompasses improvements in material selection, optimization of device design, characterization methods, and the establishment of testing standards for PSC–Si modules. In addition to these technological advancements, it is also important to have insights on the environmental impacts and benefits of the technology. This will help justify the sustainability of material choices, manufacturing processes, and design strategies for end-of-life (EOL) management, thereby facilitating their broader implementation.

A widely recognized approach for assessing environmental impacts is life cycle assessment (LCA). LCA evaluates the environmental consequences of both existing and emerging PV technologies throughout their entire life cycle, including the extraction of raw materials, manufacturing, transportation, usage, and disposal. It quantifies all the inputs (materials and energy) and outputs (emissions and wastes) across all the stages, allowing us to assess the environmental footprint of PV technologies [12–18]. LCA has been used in studies on TSC. However, these analyses were typically conducted during technology development and were based on optimal materials and conditions that contribute to the achievement of high PCE in the laboratory without necessarily considering scalability. The LCA studies were based on laboratory data, which involve processes with high energy demand and are incompatible with industrial production [19, 20]. Only one study contains an analysis of PSC–Si that includes real data from an industrial manufacturing line [21]. However, considering that PSC–Si technology is still undergoing development and might take several years before it is fully commercialized, there is a need for an evaluation of its environmental impacts from a future perspective to support its development.

To this aim, prospective LCA (pLCA) is the appropriate approach because it allows the use of multiple upscaling scenarios (foreground and background) to anticipate the environmental impact of emerging technologies at the laboratory or pilot scale, and project to a future point of mass production or use [22–26]. Few studies have evaluated the future life cycle environmental impacts of PSC–Si. Among the relevant studies published, Itten et al [27]. conducted a pLCA with a time horizon of 2025 for PSC single-junction and PSC–Si TSC. Tian et al. [28] evaluated the life cycle energy use and environmental implications of perovskite-based tandems. Similarly, Leccisi et al [29]. performed a comprehensive analysis of the energy demands and the environmental impacts of scalable perovskite-based single-junction and tandem devices. All three studies compared their results to the benchmark silicon and reported that PSC–Si exhibited lower environmental impacts compared to silicon solar cells. However, although these LCAs provided valuable inputs for decision-making, they did not account for changes that would occur in the background. To this aim, Van Der Hulst et al [30]. performed pLCA on bifacial and monofacial PSC–Si to single-junction silicon PV cells with a time scope of 2090. They reported that the environmental impacts of tandem devices decrease over time with the bifacial panels presenting a lower environmental footprint than monofacial panels. However, they did not account for changes in the tandem architecture.

This article seeks to fill this gap by applying pLCA to evaluate the environmental implications of four promising TSC architectures informed by existing literature on materials and processes suitable for industrial production. Specifically, this article considers the anticipated advancements in the TSC configurations, manufacturing processes and changes in the background processes, providing insights into the environmental consequences of producing and deploying the PSC–Si in the future. Given that the PSC subcell is still undergoing development and novel materials are being developed and improved for better efficiency and stability, future PSC–Si may incorporate different material combinations. However, a prospective assessment is also vital at this stage to identify environmental hotspots, inform sustainable design choices, and guide policymakers and manufacturers toward minimizing the environmental footprint of PSC–Si devices.

We begin by providing an overview of PSC–Si TSC technology to highlight some of the materials and advancements made in scaling up PSC–Si from laboratory to industrial scale. This is followed by a description of the prospective environmental impact assessment approach taken in this study, and finally, we present the results and conclusions.

2 | Review and Insights on the Materials Suitable for Upscaling of PSC–Si

2.1 | Materials

2T PSC–Si TSC module typically consists of two main subcells: a perovskite top cell and a silicon bottom cell [31]. The perovskite absorber layer, combined with the electron transport layer (ETL) and hole transport layer (HTL), as well as a transparent conductive oxide (TCO), forms the top PSC subcell, which

captures high-energy photons. Meanwhile, the silicon bottom subcell absorbs lower energy photons. A recombination layer or tunneling junction facilitates efficient charge transfer between the two subcells. The module is protected by encapsulating materials that shield it from environmental damage, and it features anti-reflective coatings to enhance light absorption. Additionally, an aluminum frame and junction box ensure structural integrity of the module [32]. Recently, discussions in the literature have focused on the potential pathways for future PSC–Si architectures [31, 33–37]. Various materials and configurations have been analyzed to identify alternatives suitable for industrial implementation. This section highlights some of these materials that could be adopted for the initial TSC designs on an industrial scale.

2.2 | Transparent Conductive Oxide (TCO)

The TCO functions as the front or transparent electrode, allowing electrical current to flow while also enabling the light to pass through [38]. The most common TCO material is indium tin oxide (ITO) because it provides the highest available transmittance for visible light along with the lowest electrical resistivity ($1.5–2.0\times10^{-4}\,\Omega$cm) [32]. However, ITO contains indium, which, although not considered a critical material in Europe [39], still raises global supply concerns [35]. A study by Wagner et al. [40] highlights the criticality in the supply of the resource of indium if the PSC–Si devices were to be produced at the terawatt scale. Replacing ITO with substitutes such as aluminum-doped oxide (AZO) and fluorine-doped tin oxide (FTO) may be a promising direction. Another option would be to use ultra-thin indium zinc oxide (IZO), as demonstrated by Aydin et al. [41], where they modeled a 32.5% efficient cell with a 50-nm thick IZO layer. If scaled to terawatt levels, this approach could utilize approximately 0.86 mg of indium per watt, which is still above the target of around 0.38 mg per watt necessary to meet 20% of the total indium supply [42]. Nevertheless, this approach presents a viable starting point, which, if combined with recovery and recycling efforts, could further reduce indium consumption.

2.3 | Charge Transport Layers

The polarity of the tandem device largely influences the selection of charge transport materials [33]. When the ETL of PSC is connected to the silicon bottom cell, it constitutes the NIP TSC. Conversely, when the HTL of PSC is connected to the silicon cell, it forms the PIN TSC. In the NIP-type TSC, the HTL is therefore deposited on the perovskite film, and its thickness is usually required to be sufficient to completely cover the perovskite surface to avoid direct contact between the perovskite and metal electrode [43]. Doped Spiro-OMeTAD has commonly been used as an HTL in NIP TSC, but its stability issues, complex synthesis steps, and high parasitic absorption present a barrier to its use at an industrial scale. Other alternatives that have been developed to replace Spiro-OMeTAD include the inorganic copper thiocyanate (CuSCN) and nickel oxide (NiO_x) [44], as well as the organic 2,2′,7,7-tetrakis-(N,N-di-*p*-methyl phenylamino)-9,9-spirobi-fluorene (Spiro-TTB) and poly[bis(4-phenyl)(2,4,6-trimethylphenyl)amine (PTAA). However, organic HTLs suffer from stability issues linked to their dopants, making the development of alternative dopants or dopant-free HTLs a promising pathway toward their industrial production [45]. Another strategy is to minimize the thickness of the HTL to reduce parasitic losses while ensuring proper coverage of the perovskite layer. In this regard, Spiro-TTB has been reported to be a potential substitute to Spiro-OMeTAD and its application has been demonstrated in some studies [46, 47] where the thickness was precisely controlled and uniformly coated with the evaporation technique, and the hole mobility was maintained at a high level without a dopant.

In PIN-types TSC, self-assembled monolayers (SAMS) like 2-(9H-carbazol-9-yl) ethyl) phosphonic acid (2PACZ) and its derivatives show potential as promising HTLS. Although they are expensive to produce and their performance over a large area has not been demonstrated yet, they are considered promising because they are used in small quantities [40]. Poly(3,4-ethylenedioxythiophene) polystyrene sulfonate (PEDOT:PSS) also presents as a potential HTL for PIN type TSC, considering that its industrial production is already established. However, PEDOT:PSS is acidic and may corrode the electrode in the long-term operation and reduce device stability. Additionally, the work function of PEDOT:PSS can sometimes contribute to an imperfect energy level alignment with the perovskite layer, hindering efficient hole extraction and leading to lower device performance [37].

Regarding the ETL, n-type compact or mesoporous titanium dioxide (TiO_2) is the most commonly used material in NIP PSC–Si TSC devices. However, there are several reasons to consider replacing it with tin dioxide (SnO_2). SnO_2 has higher electron mobility than TiO_2, can be obtained through a low-temperature process, and also possesses good optical band properties [48]. Furthermore, the high temperatures required in the sintering process of TiO_2 can affect the stability of the amorphous-Si:H in the bottom silicon cell, which is a significant obstacle to its commercialization. Another alternative to TiO_2 is zinc oxide (ZnO). However, despite having better conductivity and low temperature processability than TiO_2, ZnO exhibits degradation issues similar to TiO_2. Hence, SnO_2 is the favorite candidate [49].

Regarding PIN TSC, fullerene (C_{60}) and its derivatives including [6] phenyl-C61-butyric acid methyl ester (PCBM) are mostly employed as ETL. C_{60} is particularly preferred as the ETL in PIN TSC devices due to its small conduction band offset and large valence band offset compared to the perovskite. These properties enhance electron-extraction and prevent hole conduction, thereby establishing good electron-selective contact. Other advantages of C_{60} include excellent electron mobility, hydrophobic nature, and its ability to passivate perovskite surface antisite defects [50]. C_{60} has already reached an annual production in the multiton range and it appears to be feasible for use at an industrial scale from a material supply perspective [40]. However, C_{60} can suffer from morphological instability issues over time which can affect the long-term stability of the device, and it also has high parasitic absorption losses in the visible range [51]. As a result, it might not be a viable choice for industrial scale because the stability of the device is important. However, until alternatives or improvements are made, it might be the best option for now.

2.4 | Perovskite Layer

The perovskite absorber layer serves as the light-harvesting material in the top PSC subcell. Its composition, thickness, crystal form, and morphology control the photon absorption, charge

dissociation, and charge transport. The typical perovskite structure is ABX_3 where A is either organic or inorganic cations such as cesium (Cs^+), formamidine (FA^+), or methylammonium (MA^+); B is a metal (such as Pb or Sn), and X represents a halogen (mostly I and Br). Initial TSC used single-cation $MAPbI_3$, but the efficiency of the TSC devices are generally inferior because the bandgap of $MAPbI_3$ does not meet the requirements of the ideal top cell (1.73 eV) [52–54]. However, this bandgap can be tuned accordingly by modifying the composition of the material, particularly its halogens and cations. In recent TSC, double-cation perovskites such as $Cs_{0.17}FA_{0.83}Pb(Br_{0.17}I_{0.83})_3$, which incorporate two different A-site cations (such as a combination of cesium [Cs^+] and formamidinium [FA^+]), have shown improved optical absorption, thermal stability, and efficiency compared to single-cation perovskites [55]. Similarly, triple-cation perovskites, which use a mix of three A-site cations (commonly Cs^+, MA^+, and FA^+) such as $Cs_{0.05}(FA_{0.77}MA_{0.23})_{0.95}Pb(I_{0.77}Br_{0.23})_3$, offer even better stability. Moreover, triple-cation perovskite films are typically more compact and free of pinholes compared to double-cation perovskite films, and they currently present TSC with the highest efficiencies at present [56, 57]. Given their balance of efficiency and stability, the double and triple cations are expected to be key candidates for large-scale deployment of TSC. However, from the perspective of the material supply of the cations, MA and FA are considered relatively scalable, whereas Cs may be subject to supply bottlenecks [40, 58]. This scarcity of Cs could limit the ability to scale up cesium-containing perovskite films.

2.5 | Back Contact Layer

Some of the common materials used as the back electrode include gold (Au) and Silver (Ag). The high cost of Au makes it impractical for large-scale production. Ag is a more affordable alternative, although they tend to be less stable than Au and they may cause instability of the tandem device by diffusing into the perovskite and reacting with the halide to form silver halides [59]. Alternative back layer materials include copper (Cu), aluminum (Al), and carbon-based electrodes, provided they are optimized to meet the minimum conductivity requirements of the tandem device [60].

2.6 | Silicon Bottom Cell

The type of silicon cell chosen is critical as it affects the deposition methods, process temperatures, and the continuity of the top PSC. Depending on their doping type, silicon cells can be classified as p-type or n-type. In the past, p-type cells such as passivated emitter and rear cells (PERC), and aluminum back surface field cells (Al-BSF) were widely used [61]. However, n-type silicon cells like tunnel oxide passivated contact (TOPCon) cells and silicon heterojunction (SHJ) cells are gradually replacing p-type cells [62] due to their ability to obtain higher efficiency devices [63, 64].

SHJ has particularly been the preferred choice in tandem configurations because they have high operating voltages, high-efficiency potential, low-temperature coefficient, and bifacial characteristics. Moreover, the top layer in SHJ devices are TCOs, which can be applied as the recombination junction in 2T tandems with only few modifications on their thickness [65]. However, ongoing research is leading to various advancements concerning the silicon bottom cell. Future industrial PSC–Si may incorporate both p-type and n-type silicon.

2.7 | Encapsulation

In addition to the scale-up of the materials used in the production of the TSC, an equally essential step is the integration of the cells to form modules. This involves materials that provide structural support, interconnection between the cells and encapsulation. Encapsulation is necessary for perovskite-based tandem devices, which encounter stability issues due to their sensitivity to environmental factors such as moisture, oxygen, temperature, and UV radiation [66]. Furthermore, perovskite-based TSC may contain lead, which can be mitigated by encapsulation strategies such as poly(ionic liquid) (PIL)-based coatings and lead-adsorbing ionogels, which effectively sequester lead ions, preventing their release into the environment [67, 68]. Industrial encapsulation should address the stability and toxicity issues while maintaining transparency, durability, and scalability. The mainstream encapsulant material used for the silicon technology is ethyl vinyl acetate (EVA); nevertheless, it is not suitable for PSC–Si due to the high temperature used in cross-linking EVA, and during its lamination, there is the release of byproducts that are harmful to perovskites [69]. Some of the alternatives proposed in the literature include polyolefins and thermoplastic polyurethane [34].

2.8 | pLCA Methodology

This work is based on pLCA which is carried out following the four LCA phases according to the ISO standards 14040/14044 [70, 71], namely, goal and scope definition, life cycle inventory, life cycle impact assessment, and interpretation.

2.9 | Goal and Scope of Study

The goal is to assess the environmental profile of different PSC–Si TSC configurations to highlight the potential perspectives of future industrial development of this technology. The aim is to evaluate and analyze the potential changes and advancements in environmental performance over time, with the temporal scope of the analysis being 2025–2075. To take into consideration different states in the future, the analysis integrates changes to the TSC architecture to reflect material and processing scalability, forecasts of operational parameters (foreground scenarios), and modification of the electricity mix utilized in the tandem solar devices manufacturing supply chain (background scenarios). Considering the study's goal, the tandem devices will be deployed as future energy technology in a mature electricity market. Therefore, the functional unit of the analysis is 1 kWh of generated direct current electrical energy from the PV module over its lifetime. This analysis takes a cradle-to-grave approach, examining the environmental impacts of PSC–Si from the extraction of raw materials through to the fabrication of cells and modules, as well as their operation and EOL treatment. Concerning the EOL, the cut-off approach was applied, where no environmental benefit was attributed to the recovery of secondary material. Figure 1 contains a summary of the system boundaries, including changes

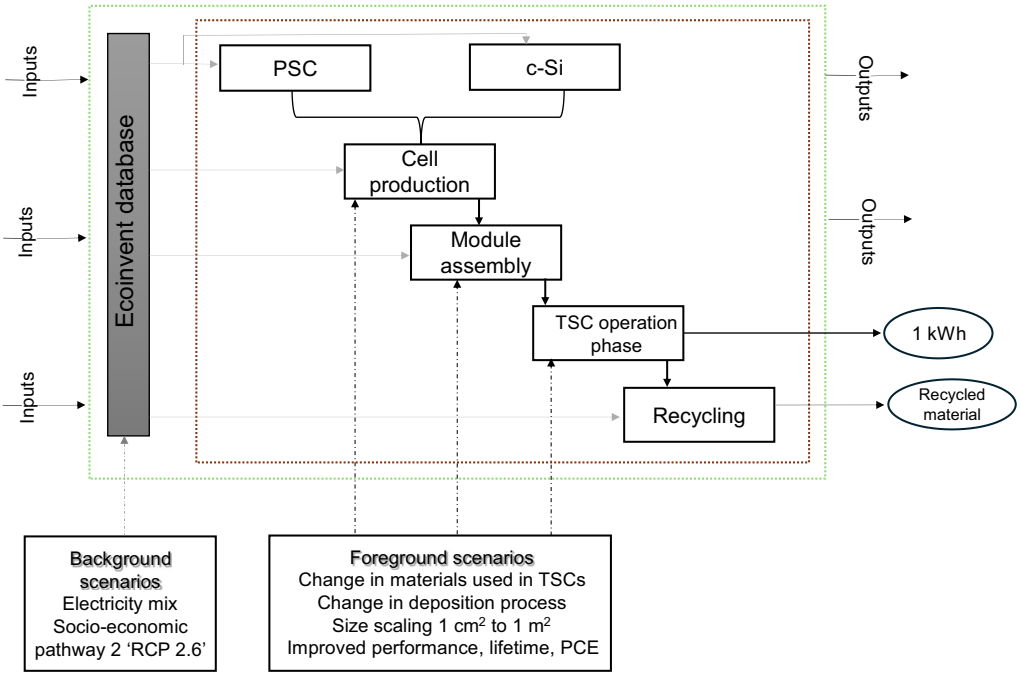

FIGURE 1 | Sketch of the system boundaries of this pLCA study, including foreground and background changes.

in foreground and background, which are explained in detail in the prospective assessment section.

2.10 | Description of the TSC Analyzed

Figure 2 shows the selected TSC designs, including the chosen materials and their respective thicknesses. The TSC 1 design features a textured silicon heterojunction (HIT Si) as the bottom subcell and Ag as the metal electrode. This configuration is analyzed as a NIP TSC, as reported in the referenced paper [47]. In this arrangement, a noninverted PSC cell is used, which includes Spiro-TTB as the HTL, a $CsFAPb(IBr)_3$ perovskite absorber layer, C_{60} for electron transport, and ITO for TCO.

TSC 2 utilizes the same HIT Si and metal electrode (Ag) as TSC 1. However, this configuration is analyzed as a PIN TSC, which includes IZO as the TCO, C_{60} as the ETL, a $CsFAPb(IBr)_3$

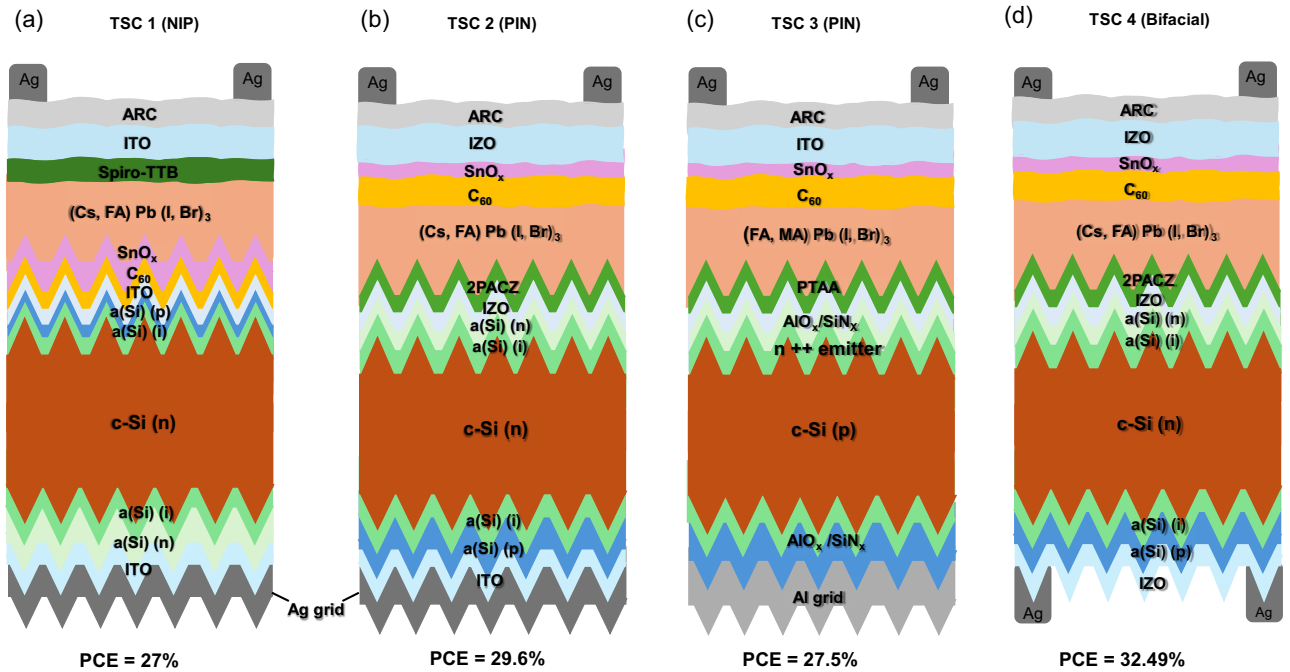

FIGURE 2 | Schematic illustration of four 2-terminal (2T) monolithic PSC–Si tandem solar cell architectures considered in this study: (TSC1) N–i–P PSC/SHJ tandem, (TSC2) P–i–N PSC/SHJ tandem, (TSC3) PSC/homojunction c-Si tandem, and (TSC4) bifacial 2T PSC/SHJ tandem [41, 47, 62, 72].

perovskite absorber layer, and 2PACZ as the HTL. Given the critical nature of indium, the TSC reported in the referenced paper employs IZO as the TCO with a reduced thickness [41], and this consideration is also taken into account in the analysis of TSC 2.

TSC 3 features a different silicon bottom cell, the PERC, and also the back metal electrode Ag is substituted with Al. Moreover, to address the concerns raised on criticality in the supply of Cs [40, 58], a different perovskite absorber layer, FAMAPbIBr, which does not contain Cs, is utilized. The fourth tandem alternative, TSC 4, is analyzed as a bifacial tandem configuration that features a 200 nm IZO thickness [73]. This is chosen to represent a grid-free large-area bifacial module configuration, for which low sheet resistance is required for efficient charge collection and can be achieved using a relatively thicker TCO [74].

In relation to the deposition process for the materials mentioned above, the energy-intensive deposition methods, such as spin-coating, were replaced by scalable techniques [75–77]. This was necessary considering that spin-coating is incompatible with large area manufacturing, and considering the textured crystalline-silicon (c-Si) bottom cells adopted in the analysis, we would require techniques that can ensure the PSC top cell are deposited in a conformal manner over large area [78, 79]. Therefore, we adopted methods such as slot-die coating for the absorber layer, ETLs and HTLs, atomic layer deposition for SnO_2, and sputtering for the TCO. It is important to note that by using slot-die coating instead of spin-coating, material losses were considered minimized and assumed to be negligible and were therefore not taken into account [80]. The next step after cell production is module assembly where we considered the P1, P2, P3 processes involved in the interconnection of the cells. Furthermore, encapsulation layers based on polyolefin (POE) and front glass are included in the analysis.

2.11 | Life Cycle Inventory (LCI)

Most of the LCI data were obtained from the literature with the Ecoinvent version 3.9.1 [81] being the primary database used for background data. Specifically, data for silicon heterojunction cells were sourced from Louwen et al. [82]. For PSC, we relied on data from studies that focused on upscaled modules [28–30, 83, 84]. However, in cases where literature data were unavailable, such as for 2PACZ and Spiro-TTB, we modeled the data based on stoichiometric equations and followed their synthesis as reported in the literature [85]. The LCIs of all processes are provided in the Supporting Information file.

The analysis of the use phase was included to assess the potential of TSC as electricity-generating devices. The electricity production was calculated in the following equation:

$$E_{\mathrm{LT}} = I \times \mathrm{PR} \times \mathrm{PD}_i \sum_{n=1}^{\mathrm{LT}} (1 - \mathrm{DR})^n \quad (1)$$

where I is the insolation (assumed to be 1700 kWh/m^2/year, which is representative of Southern Europe and the world average), PR is the performance ratio which was set to 80% as the average value [86]. $\mathrm{PD_i}$ denotes power density and was derived from literature-reported PCE [46, 72, 87, 88], under standard test conditions by normalization to 1-sun irradiance (1000 W/m^2) [64]. For the bifacial configuration TSC 4, rear-side irradiance was additionally considered by assuming a rear incident irradiance of 200 W/m^2 [89], which translates to an increased electricity output that was assumed to be 15% relative to the monofacial TSCs. Regarding the degradation rate (DR), a constant annual value of 0.9% was assumed for the perovskite (PSK) top subcell due to the lack of actual field data on their degradation rate [90], whereas the bottom Si bottom subcell was modeled with a higher first-year degradation of 1.5% followed by a lower post-DR of 0.6%, reflecting their real performance in the field [91, 92]. Regarding the LT, which is the lifetime, we assumed a lifetime of 25 years of the TSC PV system, which aligns with the industry standard average lifespan for PV panels. Given the current instability issues of the PSC top subcell, the parameters assumed for the degradation rate of the PSC top subcell and the overall lifespan of the TSC in this analysis are future projections of these parameters. However, given the uncertainty around this, a sensitivity analysis is also included.

Concerning the EOL phase, recycling is modeled in which the TSC module will be delaminated to remove the encapsulation material [93]. After which, the two subcells are separated and undergo recycling separately at different points in time. The recycling of PSC was modeled on the basis of a chemical dissolution process, and the LCI for this process was obtained from Tian et al. [94]. For the recycling of the silicon bottom cell, we derived the LCI from Latunussa et al. [95] with glass, silicon, and silver recovered as output.

2.12 | Prospective Assessment

In this section, we outline the scenarios considered for the prospective analysis. First, the foreground scenarios were developed using the framework proposed by Van Der Hulst et al. [96], which was done in three phases as outlined in Table 1. In the first phase, we assessed the technological readiness level (TRL) and maturity of the technology to identify the necessary steps for implementation within the specified timeframe. This was necessary because although silicon PV is a proven technology at TRL 9, research into its improvement and manufacturing process is ongoing. Additionally, its industrial-scale recycling process is still in development. In contrast, though PSCs have demonstrated high performance at the laboratory, they are still at the early stages of commercial deployment (low TRL ≈5) and still require further advancements. Therefore, modeling the future production and use of TSCs requires consideration of developments that will bring them to TRL 9. On the basis of literature and industry road maps [33, 35, 64], in the second phase, the changes modeled relate to fabrication methods from the current techniques used in the lab such as spin coating to scalable techniques like slot-die coating, changes in dimensions from small-area tandem cells (1 cm^2) to modules (1 m^2), as well as changes in the tandem architecture such as use of alternative materials such as Al instead of Au, 2PACZ instead of Spiro-OMeTAD [97]. For the third phase, industrial learning in the foreground system were derived from projections of the International Technology Roadmap for Photovoltaic (ITRPV) [64], where we modeled projections in lifetime, PCE and degradation rate of the TSC, as well as reduction in the amount of silver used for back contacts and the thickness of the silicon wafer from 270 μm in 2025 to the projected 100 μm in 2050 [98, 99].

TABLE 1 | Modeled projections for the TSC.

Phase: Step	Modeled changes	Current state	Target state
Phase I: Definition of the development stage	Technological development	PERC Silicon panel-TRL 9,10 HIT Silicon Monofacial tandem-TRL 4–7 Bifacial tandem-TRL 5	Industrial scale TRL 9–10
Phase II: Process changes	Scalable deposition process Use of safer solvents	Spin coating, Thermal evaporation DMF	Slot-die coating, Sputtering DMSO
	Changes in tandem architecture	Spiro-OMeTAD, Au	2-pacz, IZO, Al
	Reduction in the thickness of layers	Silicon wafer – 270 μm ITO-210 nm Silver use- 9 g/m^2	Silicon wafer – ≤100 μm IZO – 2030–50 nm, IZO - 2050 > 50 nm Silver – <2 g/m^2
Phase II: Size scaling	Product scaling	0.01 m^2	1 m^2
Phase II. Process synergies	Reduction of final waste streams	Recovery of glass, aluminum frame[3]	Recycling and recovery of Silicon, silver and ITO
Phase III: Industrial learning	Increased technological performance	Lifetime of <5 Years, Degradation rate of PSC > 6.5%, Performance ratio ≈ 75%	Lifetime = 25–30 years, Degradation rate of PSC < 2.3%, Performance ratio > 80%
Phase III: External developments	Decarbonization of electricity mix, transport and steel production	The current European electricity mix	Future European electricity mix including more renewable energy

For the background system, developments in the electricity mix used were modeled using the Python package Premise [100]. Premise utilizes data from integrated assessment model (IAM) scenarios and Ecoinvent database to update market links and technology choices. As a result, prospective LCIs (pLCIs) are generated, reflecting a future global economy under specific climate mitigation scenarios and socio-economic pathways (SSPs) [101, 102]. In this article, we relied on the data from the IAM model IMAGE [103], which follow SSP2 (also known as the "Middle of the road" pathway) and the mitigation scenario representative concentration pathway (RCP) 2.6 (limiting radiative forcing to 2.6 W/m^2 in 2100, roughly equivalent to keeping global warming below 2°C) to represent best-case possibilities [104]. From this process, the pLCIs that were generated were then combined in a superstructure database to enable practical modeling with a single database rather than multiple ones to represent all the scenarios and time steps. This superstructure database consists of an extended scenario difference file that contains variances in the flow values for all the time steps and scenarios. The scenario difference file was imported into Activity Browser [105], which is the LCA software that was used for this scenario-based analysis.

2.13 | Life Cycle Impact Assessment

In this phase, all the data collected in the LCI are converted to environmental impact indicators that provide information on the environmental performances of the TSC analyzed. For this purpose, the environmental footprint method (EF 3.1) was employed, where the environmental impacts on climate, resource depletion, air, water, and soil quality are categorized and classified into 16 midpoint categories [106]. However, this study focuses on the environmental impacts of TSC in the global warming potential (GWP) impact category because of its high level of confidence and robustness guaranteed by the Inter-governmental Panel on Climate Change (IPCC) [107]. Furthermore, GWP is relevant to highlight the effectiveness of the TSC in reducing greenhouse gas emissions throughout their life cycle in comparison to fossil fuel energy sources [108].

Moreover, the cumulative energy demand (CED), which is an LCIA method that aggregates the total energy required (both direct and indirect) during the entire life cycle of TSC, was also employed in this analysis. The evaluation of the CED allowed us to include an evaluation of the energy payback time (EPBT), which quantifies the duration needed for the TSC to generate the same amount of energy to offset all the energy input during the PV life cycle [109]. The EPBT is calculated as shown in the following equation:

$$\mathrm{EPBT} = \frac{\mathrm{CED}}{\frac{E_{\mathrm{agen}}}{\eta G} - E_{\mathrm{o\&m}}} \tag{2}$$

where E_{agen} is the annual electricity produced by the TSC, which was calculated as shown in Equation (1), ηG is the primary energy to electricity conversion efficiency, which was set to 0.31 [110]

for 2025 and increased to 0.44 [111] for 2030 and 2050 with the assumption that future electricity mix will develop to include a significant share of renewable energy sources. $E_{o\&m}$ is the annual primary energy demand for operation and maintenance, which was assumed to be zero in this analysis.

In addition to the previously mentioned indicators and focusing on GWP, we also included an analysis of the carbon payback time (CO_2PBT) to provide insights into how long it will take for the TSC to offset the GHG emissions produced throughout its life cycle. It is calculated using the following equation:

$$CO_2PBT = \frac{CCE}{E_{agen} \times E.F} \quad (3)$$

where CCE is the cumulative CO_2eq emission throughout the life cycle of TSC obtained by the GWP, E_{agen} is the annual electricity generated by the PV, which was calculated according to Equation (1) and EF is the emission factor of the grid ($kgCO_2$eq avoided per kilowatt-hour of electricity) which was set as 0.383 [112].

3 | Results and Discussion

In this section, we analyze and discuss the results of the prospective TSC configurations. As mentioned before, the prospective analysis of the four TSC configurations includes the use of materials and deposition processes that could potentially be scaled for industrial use. Additionally, we consider variations in the

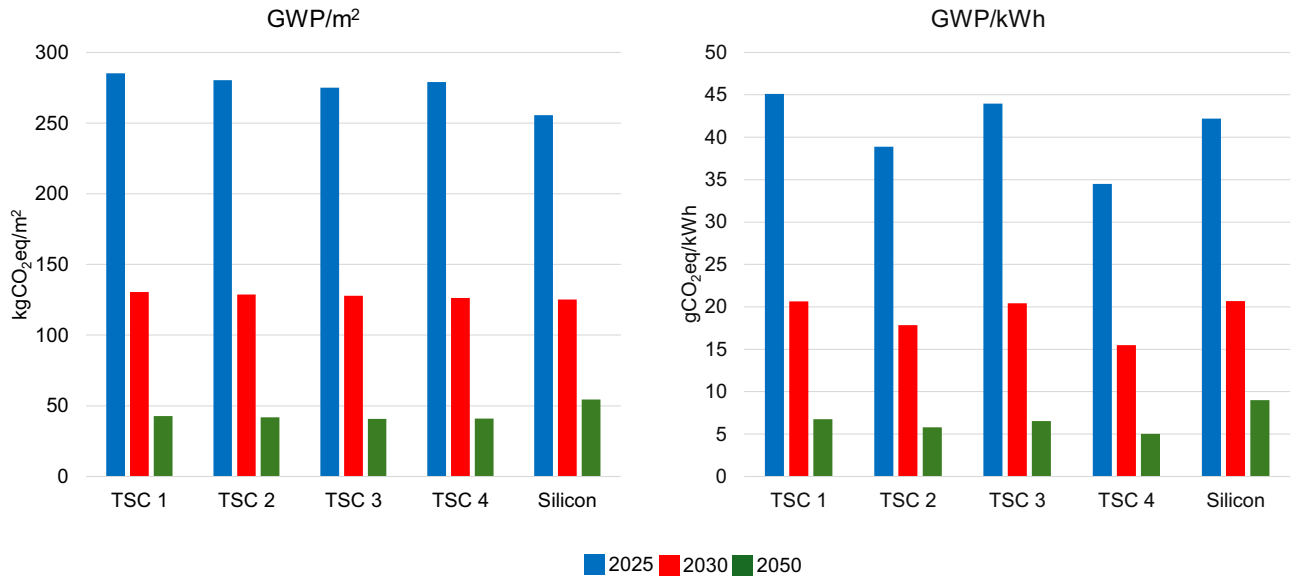

FIGURE 3 | Comparison of the GWP of four PSC–Si alternatives with Si. The years 2025, 2030, and 2050 represent years of production and the use of TSC, and the TSCs are expected to reach their EOL in 2050, 2055, and 2075, respectively.

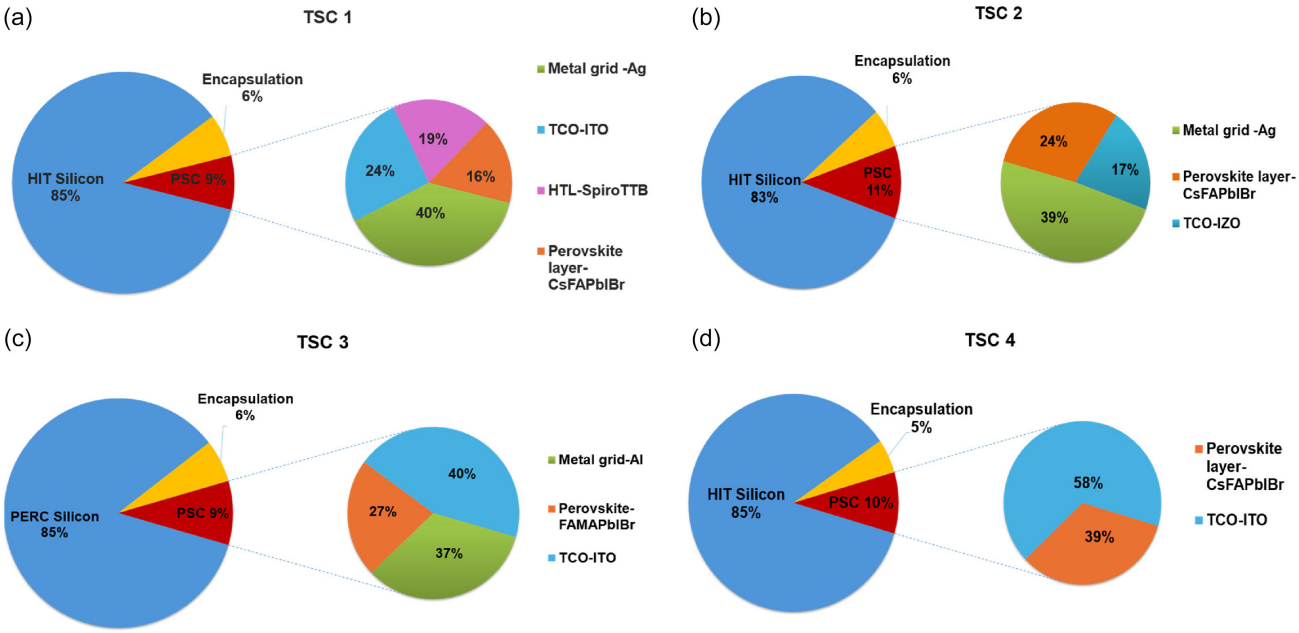

FIGURE 4 | GWP contribution analysis of the TSC architectures as of 2025.

size of the tandem cells, changes in silicon wafer thickness, and technological improvements in terms of the PCE, performance ratio, degradation rate, and overall lifetime of the TSC PV system.

The section begins with a comparison of the environmental profiles of the four TSC panels against the environmental profile of the PERC silicon module, which is taken as a reference for the current leading PV technology in the market. The initial comparison assumes a lifespan of 25 years for the TSC; where both the PSC top cell and silicon bottom cell function for 25 years. However, due to the uncertainty surrounding the lifespan of PSC cells, a sensitivity analysis regarding their lifetime and degradation rate is also included. It is noteworthy that the findings presented in this study rely on assumptions and projections that utilize the available information. Consequently, these findings carry a considerable degree of uncertainty, especially when forecasting a long period for a rapidly evolving technology. Therefore, this assessment should be viewed considering the information available today, highlighting the anticipated direction. Nonetheless, the results underscore the improvements needed in PSC–Si TSC devices to support their sustainable development.

Figure 3 illustrates the variations in the GWP of the TSC relative to that of silicon, with the bar chart on the left showing the GWP impacts of the manufacturing step of the TSC devices, whereas the bar chart on the right shows the GWP impacts per 1 kWh of electricity produced by the TSC. Generally, it is evident that the TSCs have different eco-profiles. TSC 1 has the highest GWP per kWh, primarily due to its low PCE of 27% and the materials employed in the configuration. In contrast, TSC 4 exhibits the lowest GWP/kWh. It is evident that as of 2025, the manufacturing of all the TSCs presents a higher GWP in comparison to that of silicon. However, the energy performance of the TSC devices with higher PCE, TSC 2 and TSC 4, compensates for the environmental burden of the production of the TSC compared to the single-junction silicon.

The variations in the GWP/m^2 values can be attributed to the materials employed in the tandem configurations. Specifically, by replacing ITO with IZO and reducing its thickness, as well as changing the HTL from Spiro-TTB to 2PACZ, a reduction in GWP/m^2 result is observed from 285 $kgCO_2eq/m^2$ in TSC 1 to 280 $kgCO_2$ eq/m^2 in TSC 2 in 2025. Among the tandem devices, TSC 3 shows the lowest GWP/m^2 value due to the employment of Al as the back electrode; however, the use of the materials employed in TSC 3 leads to lower PCE and, consequently, to higher GWP/kWh values when the operational phase is considered.

Figure 3 also shows that the prospective TSC designs have improved environmental performances from 2025 to 2050, with the GWP projected to decrease by approximately 70% for all the PV technologies analyzed (tandem modules and silicon). The improvements primarily stem from enhancements in the technological development identified for the prospective assessment, particularly the adoption of thinner silicon wafers and a future European electricity mix that is anticipated to incorporate a significant share of renewable sources.

An in-depth analysis of which flows contribute to the GWP profile of the TSC as of 2025 is shown in Figure 4. In agreement with previous LCA studies [17, 29], the contribution analysis shows that in the TSC configurations analyzed, the Si bottom cell contributes significantly to the GWP. This environmental impact is consistent for both types of silicon analyzed (PERC and HIT). Even with assumptions about a reduction in wafer thickness by the years 2030 and 2050, the silicon bottom cell accounts for more than 50% of the total GWP of the TSC.

Additionally, there are other materials that make a nonnegligible contribution to the GWP of the tandem configurations. Specifically, in TSC 1, significant contributions are from Ag, which is used as the back electrode, the ITO, which is used as the TCO, Spiro-TTB, and the perovskite layer. The high contribution of Ag and ITO to the GWP of TSC 1 is consistent with previous LCA studies [17, 18, 94], which show that the use of these materials have significant environmental burdens due to the high embedded energy in Ag and indium and thus high GWP.

In TSC 2, major contributions also come from Ag, IZO, and the perovskite layer. However, by changing the HTL from Spiro-TTB to 2PACZ, it is evident that HTL no longer contributes majorly to the GWP of TSC 2. Although Spiro-TTB is seen as a potential

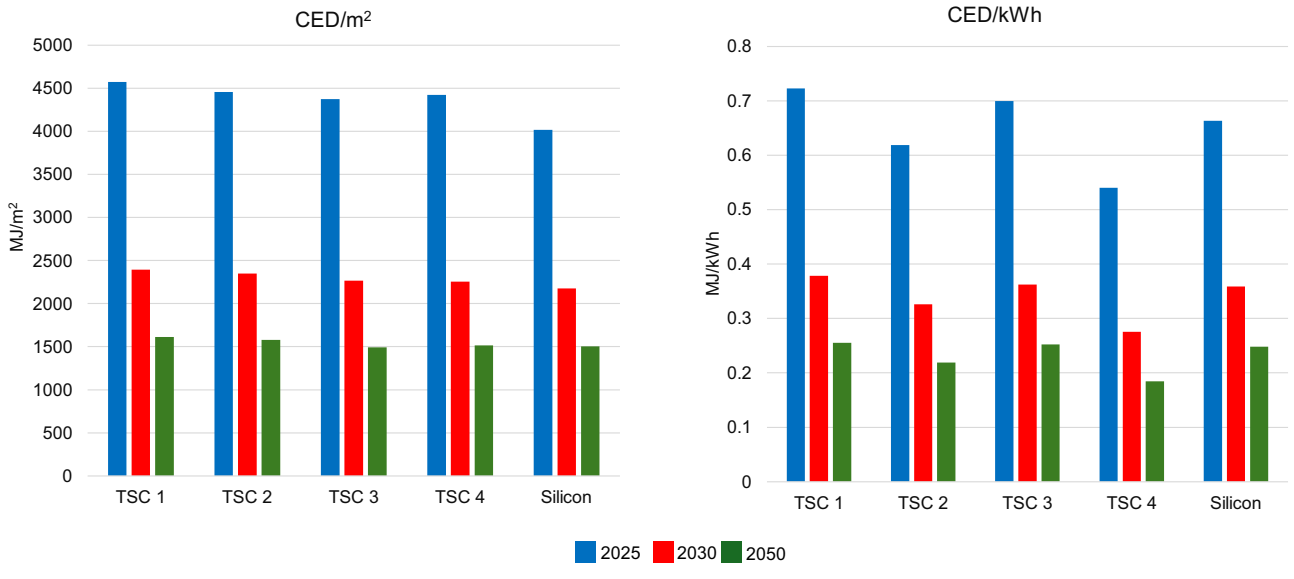

FIGURE 5 | CED of the potential TSC designs and their evolution from current state (2025) to prospective state (2030, 2050).

substitute for Spiro-OMeTAD in NIP tandem devices [36], it still is an environmental hotspot, and other alternatives should be considered.

In TSC 3, Ag was substituted with Al, and a new perovskite layer composition was used. However, as illustrated in Figure 4, the back electrode and the perovskite layer still present a significant contribution to the GWP. Al is a low-cost ideal alternative to Ag, however, the high contribution to the environmental impact in this analysis comes from the electricity used in the deposition process of the Al. Regarding the perovskite layer, both compositions have dominant contributions due to the formamidinium iodide (FAI) precursor, the impacts stem from the energy used to synthesize it [84].

The process contribution analysis of TSC 4 indicates that ITO used as the back contacting material instead of a metal electrode is one of the main contributors to the GWP of TSC 4. Although TSC 4 has a low GWP per kWh, it was modeled as a bifacial configuration containing the highest amount of ITO. From a sustainability perspective, mass production of TSC 4 would be a problem because of the criticality of indium [40]. Bifacial PSC–Si TSC solar modules present a promising opportunity for enhanced stability and energy yield compared to monofacial modules. Additionally, the bifacial module (TSC 4) analyzed in this study demonstrates better environmental performance than the monofacial modules. However, for the bifacial modules to be successfully adopted in future markets, modifications to the materials and amounts used for the TCO will be necessary.

Figure 5 illustrates the comparative analysis of the CED of the TSC designs with silicon. The first chart shows the CED of the manufacturing step of the TSC in comparison to the manufacturing of the silicon panel, whereas the second bar chart shows the CED/kWh. The results demonstrate a similar trend

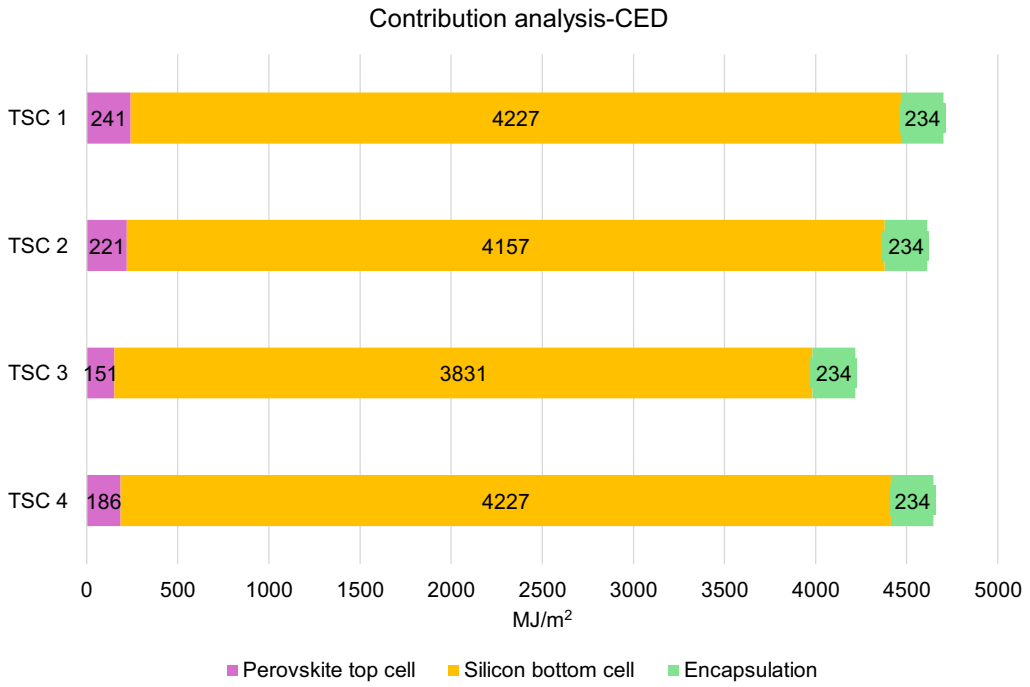

FIGURE 6 | Contribution analysis of the CED for the TSC designs.

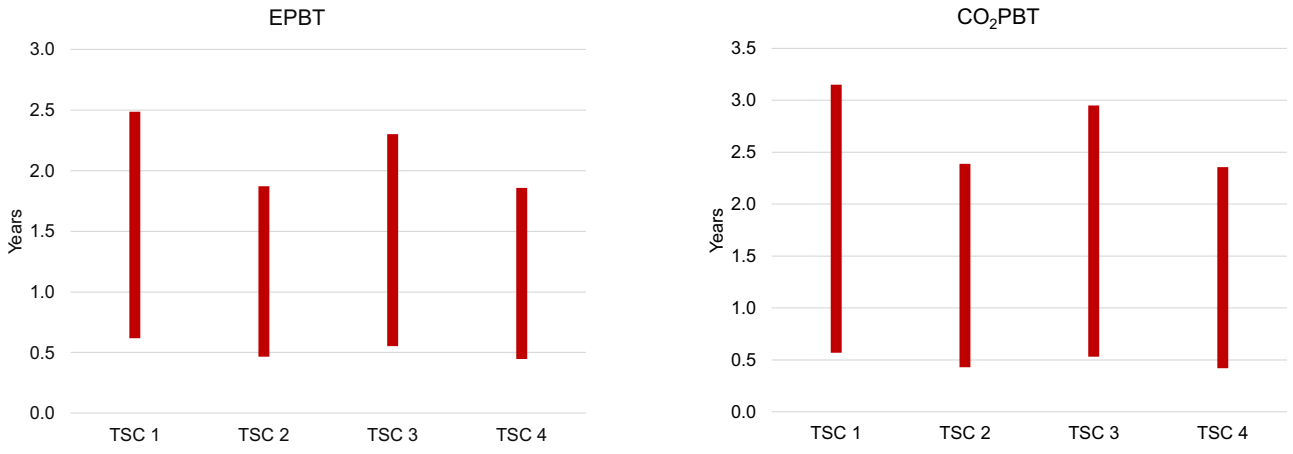

FIGURE 7 | Diagram of the EPBT and CO_2PBT indicator calculated for the TSC alternatives.

as the GWP, where TSC 1 still presents the highest CED/kWh (0.77 MJ/kWh), with TSC 4 exhibiting the lowest CED/kWh (0.57 MJ/kWh). A comparison of the CED of the manufacturing of the single-junction silicon and the TSC devices shows that the TSC presents higher CED than silicon PV due to the additional materials and energy required in the manufacturing of the TSC panels. However, the high environmental impacts are offset by the higher energy performance of the TSC panels, particularly for the bifacial module, TSC 4.

A detailed breakdown of the CED contribution as of 2025 is presented in Figure 6, where the silicon bottom cell has the largest contribution, mainly due to the energy required for silicon wafer production. Although the production of the top PSC also includes synthesis of materials that are energy-intensive, such as the precursor materials, the Si bottom remains to be the dominant contributor. However, by anticipating a reduction in silicon wafer thickness for the years 2030 and 2050, there is a general improvement in the cumulative energy requirements of the TSC, as shown in Figure 5.

On the basis of the CED and GWP results from the previous section, the calculations for EPBT and CO_2PBT are presented in Figure 7. These calculations are performed with the assumption that the TSC systems will be installed in Europe. The bar chart on the left displays the EPBT values, whereas the bar chart on the right presents the results for CO_2PBT; the top of the bars indicating the highest value, which corresponds to the EPBT and CO_2PBT

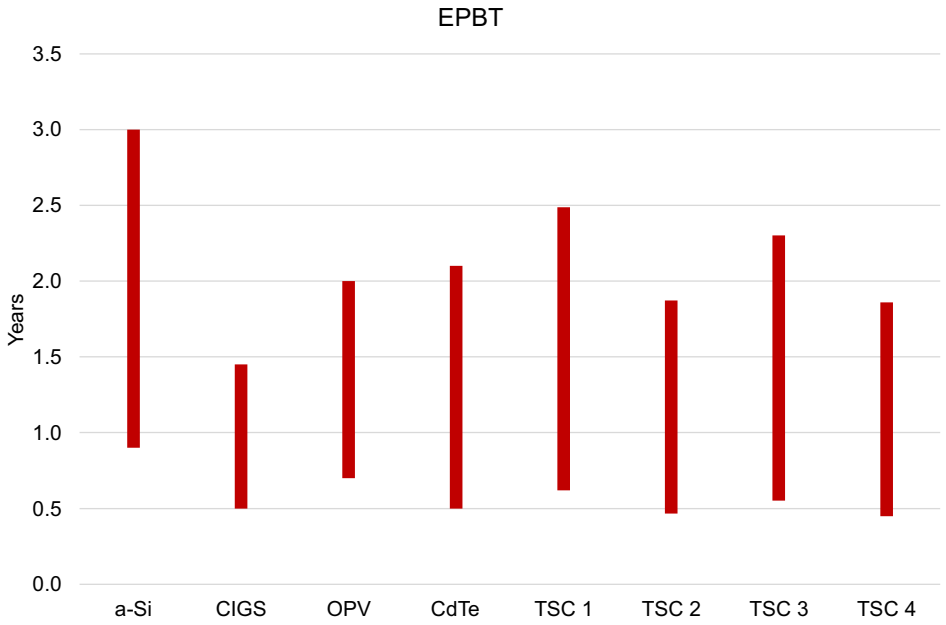

FIGURE 8 | Comparison of the EPBT values, calculated for different PV technologies [113].

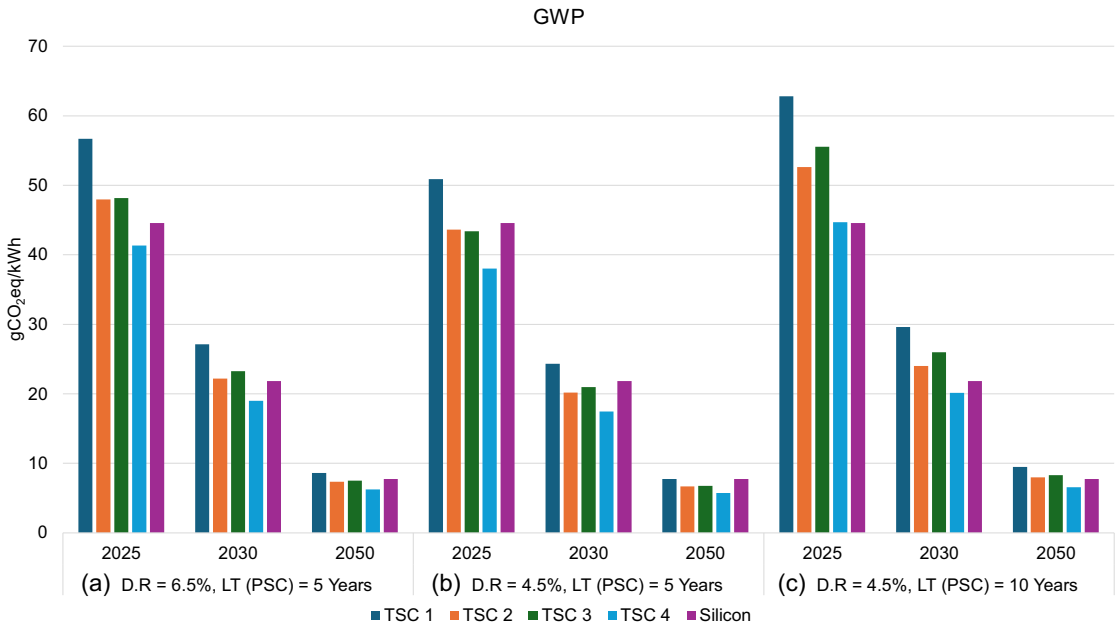

FIGURE 9 | GWP comparison with sensitivity analysis on high degradation scenarios and lifetime for PSC top subcell.

of the TSCs as of 2025, whereas the bottom of the bar shows the values corresponding to the EPBT and CO_2PBT projected for 2050.

Assuming a lifespan of 25 years and a lower degradation rate for the PSK cells, if the TSC devices are manufactured and deployed now their EPBT ranges from 1.9 years for TSC 4 to 2.5 years for TSC 1, with a projected decrease to 0.4 years (≈5 months) if they are fabricated in 2050 for TSC 4 and 0.6 years (≈7 months) for TSC 1. As shown in Figure 8, these values are comparable with the EPBT values reported in the literature for the other established PV technologies [113], showing that if the PSC–Si TSC can be developed to reach the industrial lifetime of 25 years, they will be competitive within the future PV market. The CO_2PBT of the TSC ranges from 2.3 years for TSC 4 to 3.1 years for TSC 1, with a similar projected decrease to lower values of ≈5 (TSC 4) to 7 months (TSC 1) if they are fabricated and installed in 2050.

3.1 | Sensitivity Analysis

One barrier to the commercialization of PSC-based tandem devices is the high degradation rate of the top PSC subcell, the short lifetime of which affects the overall lifetime of PSC–Si TSC devices. Various degradation rates have been reported in the literature [114] with some studies indicating that PSC–Si TSC devices may only be able to enter the market if periodic module restoration

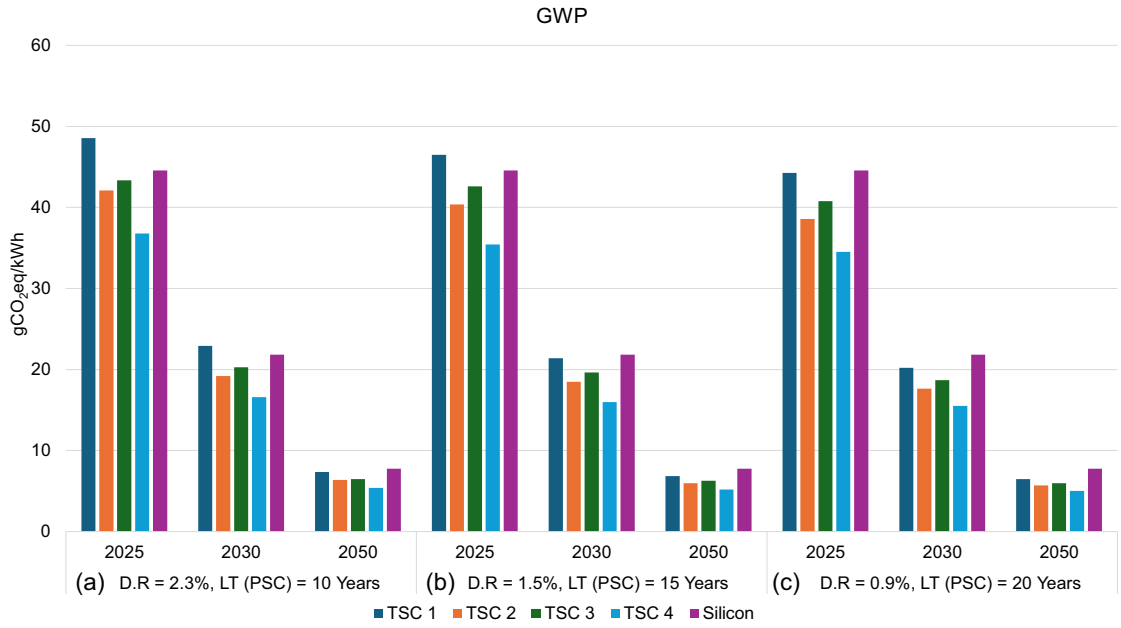

FIGURE 10 | GWP comparison with sensitivity analysis on low degradation scenarios and longer lifetime for PSC top subcell.

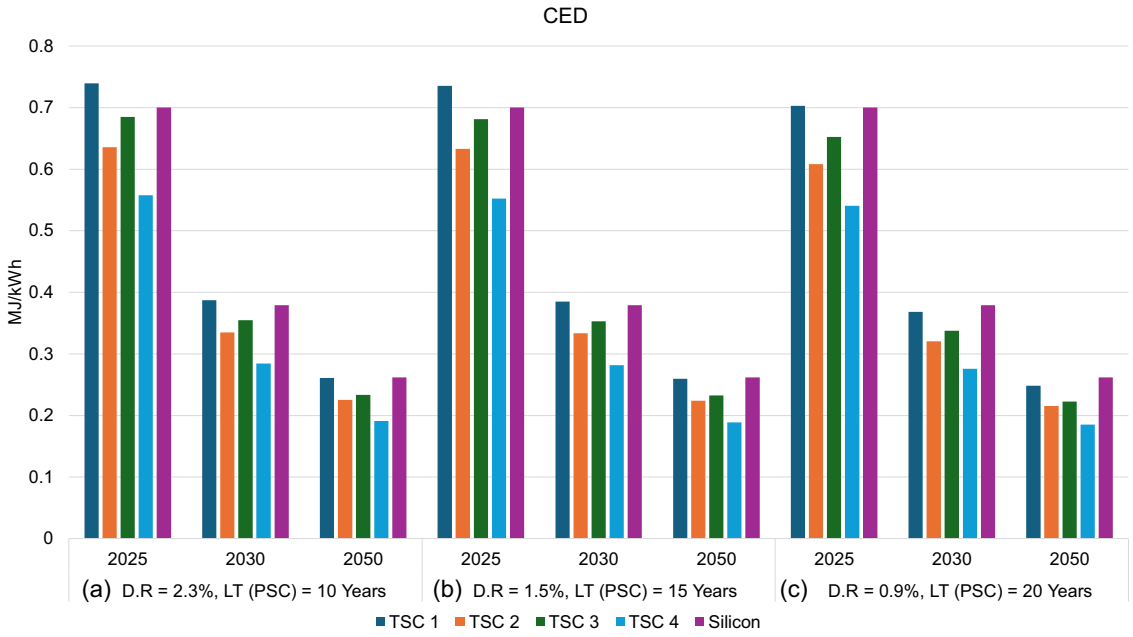

FIGURE 11 | CED comparison with sensitivity analysis on high degradation scenarios and lifetime for PSC top subcells.

is implemented to recycle and reuse the critical materials in the degraded PSC. Additionally, they need to have a degradation rate of less than 1.4% per year from the onset to be viable [115]. However, the degradation rate, as well as the lifespan of PSCs, is still subject to uncertainty.

To investigate the sensitivity of our results to these parameters, we consider different degradation rates which have a linear relationship with the lifetime of the PSC. The estimations of the degradation rates of the PSC top cell are based on estimations from Qian et al. [90], where the highest value considered is 6.5% and the lowest is 0.9%. In contrast, the degradation rate of the silicon bottom cell is set at 0.5%, as recommended by the IEA PVPS [116]. The assumption taken is that once the PSC degrades, the TSC will have to undergo delamination to remove the encapsulation material, after which the degraded PSC submodule will be removed and a new PSC submodule is placed on the existing silicon submodule [16].

A comparison of Figure 9a,b, where the degradation rate was varied while keeping lifetime constant, shows that higher degradation rates (6.5% compared to 4.5%) lead to higher GWP/kWh. This is because a faster performance decline reduces the effective energy yield over the device's lifetime, thereby increasing the GWP/kWh. Comparing parts (b) and (c) of Figure 9, where the lifetime was varied, the results show that extending the device lifetime to 10 years does not necessarily lead to lower GWP/kWh compared to a scenario with a higher degradation rate (6.5%) but shorter replacement intervals. It is also evident that despite the PSC exhibiting a high degradation rate, TSCs with higher efficiency (TSC 4) show a lower GWP compared to single-junction c-Si. However, TSCs with lower PCE, TSC 1 and TSC 3, demonstrate higher GWP than the c-Si device, even when the degraded PSCs are replaced every 5 years.

Figure 10 demonstrates that although degradation rate is a crucial parameter in the development of TSC, for values lower than 4.5, the degradation rate does not critically affect the GWP, and the sensitivity analysis doesn't show significant variations. This is highlighted by the negligible difference (≈4 gCO_2eq/kWh) between the GWP of the TSCs with the degradation rate 2.3% and those of the degradation of 0.9%. Nevertheless, it is still important that TSCs with lower PCE should have lower degradation rates to ensure that they have a lower GWP than silicon PV devices.

The results of the CED, shown in Figure 11, demonstrate a similar trend where lower degradation rates, longer lifetimes and restoration of PSC with high degradation rates contribute to environmental benefits for TSC.

4 | Conclusion

In this article, a pLCA is conducted on PSC–Si TSC modules evaluating their production and operation from the present day through to 2030 and 2050. The analysis is based on various tandem architectures identified in the literature, with a particular focus on their potential for industrial-scale production. It also considers projections of key parameters of TSC, such as operational lifetimes, cell and module efficiencies, reductions in layer thickness, and changes in future electricity mix. The study aims to identify the environmental impact hotspots associated with these tandem designs and contribute toward the sustainable development of TSC. On the basis of projected changes in TSC module design, performance, and the projections of changes in the electricity mix, the results of this prospective analysis also show that the TSC have the potential to outperform the silicon device in terms of the environmental impacts in the long-term future. In particular, the GWP of TSC are reduced by 50% in 2030 and 70% by 2050, with the CED following the same trend. The changes in the thickness of layers and silicon wafer thickness contribute to a reduction in the total EPBT, with the decarbonization of the future electricity mix contributing to a significant reduction in the CO_2PBT of the TSC. The results also highlight some hotspot materials such as the Ag back electrode, ITO, FAI precursor, and the Spiro-TTB.

The sensitivity analysis underscores the importance of high PCE for TSC. For all the environmental impacts assessed, TSC 4 was identified as the architecture with the lowest environmental profile, including CO_2PBT and EPBT. Although the high-efficiency TSCs contains hotspot materials like Ag and indium, which are still the preferred materials for high-performance PSC-based tandem, this study shows that the environmental footprint of TSC can be minimized by reducing the quantity of these hotspot materials in the tandem module and improvements in the recycling process. However, for the TSC technology to be sustainable now and in future, continued development of alternative materials will be essential.

Author Contributions

Mercy Jelagat Kipyator: data curation (lead), investigation (equal), methodology (equal), validation (equal), writing – original draft (equal), writing – review & editing (equal). **Federico Rossi**: data curation (equal), methodology (equal), writing – review & editing (equal). **Jaume-Adrià Alberola-Borràs**: investigation (equal), writing – original draft (equal), writing – review & editing (equal). **Rosario Vidal**: investigation (equal), writing – original draft (equal), writing – review & editing (equal). **Maria Laura Parisi**: conceptualization (equal), investigation (equal), supervision (lead), writing – original draft (equal), writing – review & editing (equal). **Adalgisa Sinicropi**: conceptualization (equal), project administration (lead), supervision (lead), writing – original draft (equal), writing – review & editing (equal).

Acknowledgments

M.J.K. acknowledges that parts of this research were conducted during and with the support of the Italian inter-university PhD program in sustainable development and climate change (www.phd-sdc.it). A.S., M.L.P., and M.J.K acknowledge the European Union via the project JUMP INTO SPACE (HORIZON-EIC-2023-PATHFINDERCHALLENGES-01, No. 101162377). Views and opinions expressed are however those of the authors only and do not necessarily reflect those of the European Union or the European Research Council. Neither the European Union nor the granting authority can be held responsible for them. R.V. and J.-A. A.-B. acknowledge Generalitat Valenciana (Spain) under PROMETEO Program (Q-Solutions project reference CIPROM/2021/078).

Conflicts of Interest

The authors declare no conflicts of interest.

References

1. H. H. Pourasl, R. V. Barenji, and V. M. Khojastehnezhad, "Solar Energy Status in the World: A Comprehensive Review," *Energy Reports* 10 (2023): 3474–3493.

2. J. Ramanujam, D. M. Bishop, T. K. Todorov, et al., "Flexible CIGS, CdTe and a-Si: H Based Thin Film Solar Cells: A Review," *Progress in Materials Science* 110 (2020): 100619.

3. N. Shah, A. A. Shah, P. K. Leung, et al., "A Review of Third Generation Solar Cells," *Processes* 11 (2023): 1852.

4. M. Gaëtan, V. R. Adrien, J.-W. Arnulf, Melodie de l'Epine, and IEA PVPS Task 1 members, *Snapshot of Global PV Markets* (IEA PVPS, 2025).

5. F. Khan, B. D. Rezgui, M. T. Khan, and F. Al-Sulaiman, "Perovskite-Based Tandem Solar Cells: Device Architecture, Stability, and Economic Perspectives," *Renewable and Sustainable Energy Reviews* 165 (2022): 112553.

6. S.-P. Feng, Y. Cheng, H.-L. Yip, et al., "Roadmap on Commercialization of Metal Halide Perovskite Photovoltaics," *Journal of Physics: Materials* 6 (2023): 032501.

7. L. Dai, S. Li, Y. Hu, et al., "Three-Terminal Monolithic Perovskite/Silicon Tandem Solar Cell Exceeding 29% Power Conversion Efficiency," *ACS Energy Letters* 8 (2023): 3839–3842.

8. D. Khodair, A. Saeed, A. Shaker, M. Abouelatta, O. A. M. Abdelraouf, and S. EL-Rabaie, "A Review on Tandem Solar Cells Based on Perovskite/Si:2-T Versus 4-T Configurations," *Solar Energy* 300 (2025): 113815.

9. National Laboratory of the Rockies, Best Research-Cell Efficiency Chart (Golden, CO, USA, 2025), https://www.nlr.gov/pv/cell-efficiency.

10. M. A. Green, E. D. Dunlop, M. Yoshita, et al., "Solar Cell Efficiency Tables (Version 67)," *Progress in Photovoltaics* 34 (2026): 482, pip.70068.

11. C. U. Kim, E. D. Jung, Y. W. Noh, et al., "Strategy for Large-Scale Monolithic Perovskite /Silicon Tandem Solar Cell: A Review of Recent Progress," *EcoMat* 3 (2021): e12084.

12. A. Laurent, N. Espinosa, and M. Z. Hauschild, *Life in Cycle Assessment*, ed. M. Z. Hauschild, R. K. Rosenbaum, and S. I. Olsen (Springer International Publishing, 2018), pp. 633–668.

13. S. Maranghi, M. L. Parisi, R. Basosi, and A. Sinicropi, "Environmental Profile of the Manufacturing Process of Perovskite Photovoltaics: Harmonization of Life Cycle Assessment Studies," *Energies* 12 (2019): 3746.

14. A. Urbina, "Sustainability of Photovoltaic Technologies in Future Net-Zero Emissions Scenarios," *Progress in Photovoltaics* 31 (2023): 1255–1269.

15. M. L. Parisi and A. Sinicropi, "Closing the Loop for Perovskite Solar Modules," *Nature Sustainability* 4 (2021): 754–755.

16. M. J. Kipyator, F. Rossi, M. L. Parisi, et al., "Scenario-Based Recycling Strategies for Perovskite-Silicon Tandem Solar Cells: A Harmonized Life Cycle Assessment Study," *Sustainable Energy & Fuels* 8 (2024): 2570–2582.

17. I. Celik, A. B. Phillips, Z. Song, et al., "Environmental Science Environmental Analysis of Perovskites and Other Relevant Solar Cell Technologies in a Tandem," *Energy & Environmental Science* 10 (2017): 1874–1884.

18. M. Monteiro Lunardi, A. Wing Yi Ho-Baillie, J. P. Alvarez-Gaitan, S. Moore, and R. Corkish, "A Life Cycle Assessment of Perovskite/Silicon Tandem Solar Cells: Perovskite/Silicon Tandem Solar Cell *LCA*," *Progress in Photovoltaics: Research and Applications* 25 (2017): 679–695.

19. R. Vidal, J. Alberola-Borràs, N. Sánchez-Pantoja, and I. Mora-Seró, "Comparison of Perovskite Solar Cells with Other Photovoltaics Technologies from the Point of View of Life Cycle Assessment," *Advanced Energy and Sustainability Research* 2 (2021): 2000088.

20. F. Rossi, M. Jelagat Kipyator, T. Aernouts, et al., "Unveiling the Potential of Perovskite Solar Systems in Building Integrated Installations: A Consequential and Prospective Life Cycle Assessment and Economic Analysis," *Energy and Buildings* 312 (2024): 114214.

21. M. Roffeis, S. Kirner, J. C. Goldschmidt, et al., "Correction: New Insights into the Environmental Performance of Perovskite-on-Silicon Tandem Solar Cells – a Life Cycle Assessment of Industrially Manufactured Modules," *Sustainable Energy Fuels* 6 (2022): 4102–4102.

22. S. Cucurachi, C. Van Der Giesen, and J. Guinée, "Ex-Ante LCA of Emerging Technologies," *Procedia CIRP* 69 (2018): 463–468.

23. B. Steubing, A. Mendoza Beltran, and R. Sacchi, "Conditions for the Broad Application of Prospective Life Cycle Inventory Databases," *The International Journal of Life Cycle Assessment* 28 (2023): 1092–1103.

24. S. M. Moni, R. Mahmud, K. High, and M. Carbajales-Dale, "Life Cycle Assessment of Emerging Technologies: A Review," *Journal of Industrial Ecology* 24 (2020): 52–63.

25. M. A. Charalambous, R. Sacchi, V. Tulus, and G. Guillén-Gosálbez, "Integrating Emerging Technologies Deployed at Scale Within Prospective Life Cycle Assessments," *Sustainable Production and Consumption* 50 (2024): 499–510.

26. R. Arvidsson, A. Tillman, B. A. Sandén, et al., "Environmental Assessment of Emerging Technologies: Recommendations for Prospective LCA," *Journal of Industrial Ecology* 22 (2018): 1286–1294.

27. R. Itten and M. Stucki, "Highly Efficient 3rd Generation Multi-Junction Solar Cells Using Silicon Heterojunction and Perovskite Tandem: Prospective Life Cycle Environmental Impacts," *Energies* 10 (2017): 841.

28. X. Tian, S. D. Stranks, and F. You, "Life Cycle Energy use and Environmental Implications of High-Performance Perovskite Tandem Solar Cells," *Science Advances* 6 (2020): eabb0055.

29. E. Leccisi and V. Fthenakis, "Life Cycle Energy Demand and Carbon Emissions of Scalable Single-Junction and Tandem Perovskite PV," *Progress in Photovoltaics* 29 (2021): 1078–1092.

30. M. K. Van Der Hulst, D. Magoss, Y. Massop, et al., "Comparing Environmental Impacts of Single-Junction Silicon and Silicon/Perovskite Tandem Photovoltaics–A Prospective Life Cycle Assessment," *ACS Sustainable Chemistry & Engineering* 12 (2024): 8860–8870.

31. R. A. Afre and D. Pugliese, "Perovskite Solar Cells: A Review of the Latest Advances in Materials, Fabrication Techniques, and Stability Enhancement Strategies," *Micromachines* 15 (2024): 192.

32. H. Li and W. Zhang, "Perovskite Tandem Solar Cells: From Fundamentals to Commercial Deployment," *Chemical Reviews* 120 (2020): 9835–9950.

33. E. Aydin, T. G. Allen, M. De Bastiani, et al., "Pathways toward Commercial Perovskite/Silicon Tandem Photovoltaics," *Science* 383 (2024): eadh3849.

34. K. J. Prince, H. M. Mirletz, E. A. Gaulding, et al., "Sustainability Pathways for Perovskite Photovoltaics," *Nature Materials* 24 (2024): 22.

35. X. Tian, S. D. Stranks, J. Huang, V. M. Fthenakis, Y. Yang, and F. You, "Perspectives for Sustainability Analysis of Scalable Perovskite Photovoltaics," *Energy & Environmental Science* 18 (2025): 194–213.

36. Y. Shi, J. J. Berry, and F. Zhang, "Perovskite/Silicon Tandem Solar Cells: Insights and Outlooks," *ACS Energy Letters* 9 (2024): 1305–1330.

37. S. Akhil, S. Akash, A. Pasha, et al., "Review on Perovskite Silicon Tandem Solar Cells: Status and Prospects 2T, 3T and 4T for Real World Conditions," *Materials and Design* 211 (2021): 110138.

38. Y. Dong, R. Yu, G. Su, et al., "Interface Reactive Sputtering of Transparent Electrode for High-Performance Monolithic and Stacked Perovskite Tandem Solar Cells," *Advanced Materials* 36 (2024): 2312704.

39. European Commission: Directorate-General for Internal Market, Industry, *Entrepreneurship and SMEs, Study on the critical raw materials for the EU 2023 – Final report* (Publications Office of the European Union, 2023), https://data.europa.eu/doi/10.2873/725585.

40. L. Wagner, J. Suo, B. Yang, et al., "The Resource Demands of Multi-Terawatt-Scale Perovskite Tandem Photovoltaics," *Joule* 8 (2024): 1142–1160.

41. E. Aydin, E. Ugur, B. K. Yildirim, et al., "Enhanced Optoelectronic Coupling for Perovskite/Silicon Tandem Solar Cells," *Nature* 623 (2023): 732–738.

42. Y. Zhang, M. Kim, L. Wang, P. Verlinden, and B. Hallam, "Design Considerations for Multi-Terawatt Scale Manufacturing of Existing and Future Photovoltaic Technologies: Challenges and Opportunities Related to Silver, Indium and Bismuth Consumption," *Energy & Environmental Science* 14 (2021): 5587–5610.

43. C. Zhang, K. Wei, J. Hu, et al., "A Review on Organic Hole Transport Materials for Perovskite Solar Cells: Structure, Composition and Reliability," *Materials Today* 67 (2023): 518–547.

44. F. Hou, X. Ren, H. Guo, et al., "Monolithic Perovskite/Silicon Tandem Solar Cells: A Review of the Present Status and Solutions toward Commercial Application," *Nano Energy* 124 (2024): 109476.

45. F. M. Rombach, S. A. Haque, and T. J. Macdonald, "Lessons Learned from Spiro-OMeTAD and PTAA in Perovskite Solar Cells," *Energy & Environmental Science* 14 (2021): 5161–5190.

46. F. Sahli, J. Werner, B. A. Kamino, et al., "Fully Textured Monolithic Perovskite/Silicon Tandem Solar Cells with 25.2% Power Conversion Efficiency," *Nature Mater* 17 (2018): 820–826.

47. E. Aydin, J. Liu, E. Ugur, et al., "Ligand-Bridged Charge Extraction and Enhanced Quantum Efficiency Enable Efficient n–i–p Perovskite/Silicon Tandem Solar Cells," *Energy & Environmental Science* 14 (2021): 4377–4390.

48. S. Zheng, G. Wang, T. Liu, L. Lou, S. Xiao, and S. Yang, "Materials and Structures for the Electron Transport Layer of Efficient and Stable Perovskite Solar Cells," *Science China Chemistry* 62 (2019): 800–809.

49. J. Burschka, N. Pellet, S.-J. Moon, et al., "Sequential Deposition as a Route to High-Performance Perovskite-Sensitized Solar Cells," *Nature* 499 (2013): 316–319.

50. A. A. Said, E. Aydin, E. Ugur, et al., "Sublimed C60 for Efficient and Repeatable Perovskite-Based Solar Cells," *Nature Communications* 15 (2024): 708.

51. M. De Bastiani, G. Armaroli, R. Jalmood, et al., "Mechanical Reliability of Fullerene/Tin Oxide Interfaces in Monolithic Perovskite/Silicon Tandem Cells," *ACS Energy Letters* 7 (2022): 827–833.

52. S. Albrecht, M. Saliba, J.-P. Correa-Baena, et al., "Towards Optical Optimization of Planar Monolithic Perovskite/Silicon-Heterojunction Tandem Solar Cells," *Journal of Optics* 18 (2016): 064012.

53. J. P. Mailoa, C. D. Bailie, E. C. Johlin, et al., "A. 2-Terminal Perovskite/Silicon Multijunction Solar Cell Enabled by a Silicon Tunnel Junction," *Applied Physics Letters* 106 (2015): 121105.

54. B. Chen, Y. Bai, Z. Yu, et al., "Efficient Semitransparent Perovskite Solar Cells for 23.0%-Efficiency Perovskite/Silicon Four-Terminal Tandem Cells," *Advanced Energy Materials* 6 (2016): 1601128.

55. M. M. Byranvand, C. Otero-Martínez, J. Ye, et al., "Recent Progress in Mixed A-Site Cation Halide Perovskite Thin-Films and Nanocrystals for Solar Cells and Light-Emitting Diodes," *Advanced Optical Materials* 10 (2022): 2200423.

56. S. S. Mali, J. V. Patil, D. W. Park, Y. H. Jung, and C. K. Hong, "Intrinsic and Extrinsic Stability of Triple-Cation Perovskite Solar Cells through Synergistic Influence of Organic Additive," *Cell Reports Physical Science* 3 (2022): 100906.

57. Y. Sun, J. Peng, Y. Chen, Y. Yao, and Z. Liang, "Triple-Cation Mixed-Halide Perovskites: Towards Efficient, Annealing-Free and Air-Stable Solar Cells Enabled by Pb(SCN)2 Additive," *Scientific Reports* 7 (2017): 46193.

58. R. Vidal, J.-A. Alberola-Borràs, and I. Mora-Seró, "Abiotic Depletion and the Potential Risk to the Supply of Cesium," *Resources Policy* 68 (2020): 101792.

59. L. Duan, D. Walter, N. Chang, et al., "Stability Challenges for the Commercialization of Perovskite–silicon Tandem Solar Cells," *Nature Reviews Materials* 8 (2023): 261–281.

60. A. U. Rehman, E. P. Van Kerschaver, E. Aydin, W. Raja, T. G. Allen, and S. De Wolf, "Electrode Metallization for Scaled Perovskite/Silicon Tandem Solar Cells: Challenges and Opportunities," *Progress in Photovoltaics* 31 (2023): 429–442.

61. T. G. Allen, J. Bullock, X. Yang, A. Javey, and S. De Wolf, "Passivating Contacts for Crystalline Silicon Solar Cells," *Nature Energy* 4 (2019): 914–928.

62. C. Messmer, B. S. Goraya, S. Nold, et al., "The Race for the Best Silicon Bottom Cell: Efficiency and Cost Evaluation of Perovskite–silicon Tandem Solar Cells," *Progress in Photovoltaics* 29 (2021): 744–759.

63. W. Chi, S. K. Banerjee, K. G. D. I. Jayawardena, S. R. P. Silva, and S. I. Seok, "Perovskite/Silicon Tandem Solar Cells: Choice of Bottom Devices and Recombination Layers," *ACS Energy Letters* 8 (2023): 1535–1550.

64. VDMA (Photovoltaic Equipment), International Technology Roadmap for Photovoltaic (ITRPV): 2023 Results, 15th ed. (VDMA, 2024).

65. J. Zheng, W. Duan, Y. Guo, et al., "Efficient Monolithic Perovskite–Si Tandem Solar Cells Enabled by an Ultra-Thin Indium Tin Oxide Interlayer," *Energy & Environmental Science* 16 (2023): 1223–1233.

66. B. P. Kore, M. Jamshidi, and J. M. Gardner, "The Impact of Moisture on the Stability and Degradation of Perovskites in Solar Cells," *Materials Advances* 5 (2024): 2200–2217.

67. H. Chen, G.-H. Zhang, Q.-H. Zhu, et al., "Lead Sequestration in Perovskite Photovoltaic Device Encapsulated with Water-Proof and Adhesive Poly(ionic Liquid," *ACS Applied Materials & Interfaces* 15 (2023): 13637–13643.

68. X. Xiao, M. Wang, S. Chen, et al., "Lead-Adsorbing Ionogel-Based Encapsulation for Impact-Resistant, Stable, and Lead-Safe Perovskite Modules," *Science Advances* 7 (2021): eabi8249.

69. M. De Bastiani, M. Babics, E. Aydin, A. S. Subbiah, L. Xu, and S. De Wolf, "All Set for Efficient and Reliable Perovskite/Silicon Tandem Photovoltaic Modules?," *Solar RRL* 6 (2022): 2100493.

70. International Standards Organisation. ISO 14040: 2006 Environmental Management – Life Cycle Assessment – Principles and Guidelines, Geneva, Switzerland, 2006.

71. International Standards Organisation. ISO 14044:2006 Environmental Management – Life Cycle Assessment – Requirements and Guidelines, Geneva, Switzerland, 2006.

72. H. Hao, S.-T. Zhang, K. Wang, et al., "Energy Yield Prediction of Bifacial Perovskite/Silicon Tandem Photovoltaic Modules," *Solar RRL* 7 (2023): 2300218.

73. K. Liu, A. A. Miskevich, V. A. Loiko, et al., "Interference Effects Induced by Electrodes and Their Influences on the Distribution of Light Field in Perovskite Absorber and Current Matching of Perovskite/Silicon Tandem Solar Cell," *Solar Energy* 252 (2023): 252–259.

74. M. R. Golobostanfard, M. Othman, D. Turkay, et al., "Bifacial Perovskite/Silicon Heterojunction Tandem Solar Cells Based on FAPbI3-Based Perovskite via Hybrid Evaporation-Spin Coating," *Nano Energy* 131 (2024): 110269.

75. A. Agresti, F. Di Giacomo, S. Pescetelli, and A. Di Carlo, "Scalable Deposition Techniques for Large-Area Perovskite Photovoltaic Technology: A Multi-Perspective Review," *Nano Energy* 122 (2024): 109317.

76. F. Rossi, L. Rotondi, M. Stefanelli, A. Sinicropi, L. Vesce, and M. L. Parisi, "Comparative Life Cycle Assessment of Different Fabrication Processes for Perovskite Solar Mini-Modules," *EPJ Photovolt* 15 (2024): 20.

77. L. Vesce, M. Stefanelli, F. Rossi, et al., "Perovskite Solar Cell Technology Scaling-up: Eco-Efficient and Industrially Compatible Sub-Module

Manufacturing by Fully Ambient Air Slot-Die/Blade Meniscus Coating," *Progress in Photovoltaics* 32 (2024): 115–129.

78. B. P. Kore, O. Er-raji, O. Fischer, et al., "Efficient Fully Textured Perovskite Silicon Tandems with Thermally Evaporated Hole Transporting Materials," *Energy & Environmental Science* 18 (2025): 354–366.

79. M. Vasilopoulou, D. Huang, J. Gong, et al., "Tandem Takeoff: Powering Tomorrow with Industrial-Grade Perovskite/Silicon Solar Cells," *Advanced Energy Materials* 16 (2026): e04478.

80. Z. Liu, D. He, Y. Yu, X. Liu, X. Shai, and J. Chen, "Slot-Die Coating Deposition Method in High-Performance Perovskite Solar Modules," *Solar RRL* 9 (2025): 2400824.

81. Ecoinvent database, version 3.9.1 (Ecoinvent Association, Zürich, Switzerland, 2022), https://v391.ecoquery.ecoinvent.org/.

82. A. Louwen, W. G. J. H. M. Van Sark, R. E. I. Schropp, W. C. Turkenburg, and A. P. C. Faaij, "Life-Cycle Greenhouse Gas Emissions and Energy Payback Time of Current and Prospective Silicon Heterojunction Solar Cell Designs," *Progress in Photovoltaics* 23 (2015): 1406–1428.

83. S. A. Khalifa, S. Spatari, A. T. Fafarman, and J. B. Baxter, "Environmental Sustainability of Mixed Cation Perovskite Materials in Photovoltaics Manufacturing," *ACS Sustainable Chemistry & Engineering* 8 (2020): 16537–16548.

84. J.-A. Alberola-Borràs, R. Vidal, and I. Mora-Seró, "Evaluation of Multiple Cation/Anion Perovskite Solar Cells through Life Cycle Assessment," *Sustainable Energy Fuels* 2 (2018): 1600–1609.

85. F. Piccinno, R. Hischier, S. Seeger, and C. Som, "From Laboratory to Industrial Scale: A Scale-up Framework for Chemical Processes in Life Cycle Assessment Studies," *Journal of Cleaner Production* 135 (2016): 1085–1097.

86. Fraunhofer Institute for Solar Energy Systems ISE, Photovoltaics Report (Freiburg, Germany, 2025), https://www.ise.fraunhofer.de/.

87. B. Chen, P. Wang, R. Li, et al., "A Two-Step Solution-Processed Wide-Bandgap Perovskite for Monolithic Silicon-Based Tandem Solar Cells with >27% Efficiency," *ACS Energy Letters* 7 (2022): 2771–2780.

88. L. Mao, T. Yang, H. Zhang, et al., "Fully Textured, Production-Line Compatible Monolithic Perovskite/Silicon Tandem Solar Cells Approaching 29% Efficiency," *Advanced Materials* 34 (2022): 2206193.

89. M. De Bastiani, A. S. Subbiah, M. Babics, et al., "Bifacial Perovskite/Silicon Tandem Solar Cells," *Joule* 6 (2022): 1431–1445.

90. J. Qian, M. Ernst, N. Wu, and A. Blakers, "Impact of Perovskite Solar Cell Degradation on the Lifetime Energy Yield and Economic Viability of Perovskite/Silicon Tandem Modules," *Sustainable Energy and Fuels* 3 (2019): 1439–1447.

91. S. Herceg, I. Kaaya, J. Ascencio-Vásquez, M. Fischer, K.-A. Weiß, and L. Schebek, "The Influence of Different Degradation Characteristics on the Greenhouse Gas Emissions of Silicon Photovoltaics: A Threefold Analysis," *Sustainability* 14 (2022): 5843.

92. M. Theristis, J. S. Stein, C. Deline, et al., "Onymous Early-Life Performance Degradation Analysis of Recent Photovoltaic Module Technologies," *Progress in Photovoltaics* 31 (2023): 149–160.

93. G. Yang, M. Wang, C. Fei, et al., "Recycling Silicon Bottom Cells from End-of-Life Perovskite–Silicon Tandem Solar Cells," *ACS Energy Letters* 8 (2023): 1639–1644.

94. X. Tian, S. D. Stranks, and F. You, "Life Cycle Assessment of Recycling Strategies for Perovskite Photovoltaic Modules," *Nature Sustainability* 4 (2021): 821–829.

95. C. E. L. Latunussa, F. Ardente, G. A. Blengini, and L. Mancini, "Life Cycle Assessment of an Innovative Recycling Process for Crystalline Silicon Photovoltaic Panels," *Solar Energy Materials and Solar Cells* 156 (2016): 101–111.

96. M. K. Van Der Hulst, M. A. J. Huijbregts, N. Van Loon, et al., "A Systematic Approach to Assess the Environmental Impact of Emerging Technologies: A Case Study for the GHG Footprint of CIGS Solar Photovoltaic Laminate," *Journal of Industrial Ecology* 24 (2020): 1234–1249.

97. R. Frischknecht, I. Itten, F. Wyss, et al., *Life Cycle Assessment of Future Photovoltaic Electricity Production from Residential-Scale Systems Operated in Europe* (IEA PVPS Task 12, Report T12-19:2020, 2020), https://iea-pvps.org/.

98. D. Cheng and Y. Gao, "A Critical Review on the Fracture of Ultra-Thin Photovoltaics Silicon Wafers," *Solar Energy Materials and Solar Cells* 274 (2024): 112999.

99. U. Chime, W. Duan, A. Lambertz, et al., "Thin Silicon Heterojunction Solar Cells in Perovskite Shadow: Bottom Cell Prospective," *Solar Energy Materials and Solar Cells* 270 (2024): 112813.

100. R. Sacchi, T. Terlouw, K. Siala, et al., "PRospective EnvironMental Impact asSEment (premise): A Streamlined Approach to Producing Databases for Prospective Life Cycle Assessment Using Integrated Assessment Models," *Renewable and Sustainable Energy Reviews* 160 (2022): 112311.

101. A. Mendoza Beltran, B. Cox, C. Mutel, et al., "When the Background Matters: Using Scenarios from Integrated Assessment Models in Prospective Life Cycle Assessment," *Journal of Industrial Ecology* 24 (2020): 64–79.

102. K. Riahi, D. P. Van Vuuren, E. Kriegler, et al., "The Shared Socioeconomic Pathways and Their Energy, Land use, and Greenhouse Gas Emissions Implications: An Overview," *Global Environmental Change* 42 (2017): 153–168.

103. S. Elke, T. Kram Detlef van Vuuren, and L. Bouwman, Integrated Assessment of Global Environmental Change with IMAGE 3.0 (2014).

104. T. Weidner, V. Tulus, and G. Guillén-Gosálbez, "Environmental Sustainability Assessment of Large-Scale Hydrogen Production Using Prospective Life Cycle Analysis," *International Journal of Hydrogen Energy* 48 (2023): 8310–8327.

105. B. Steubing, D. De Koning, A. Haas, and C. L. Mutel, "The Activity Browser—An Open Source LCA Software Building on Top of the Brightway Framework," *Software Impacts* 3 (2020): 100012.

106. European Commission Joint Research Centre, Updated Characterisation and Normalisation Factors for the Environmental Footprint 3.1 Method (Publications Office, 2023).

107. K. Luana, R. Frischknecht, P. Stolz, and Sinha Parikhit, Environmental Life Cycle Assessment of Residential PV and Battery Storage Systems (n.d.).

108. *International Reference Life Cycle Data System (ILCD) Handbook: General Guide for Life Cycle Assessment: Provisions and Action Steps*, ed. European Commission (Publications Office, 2011).

109. R. Frischknecht, F. Wyss, S. Büsser Knöpfel, T. Lützkendorf, and M. Balouktsi, "Cumulative Energy Demand in LCA: The Energy Harvested Approach," *The International Journal of Life Cycle Assessment* 20 (2015): 957–969.

110. M. L. Parisi, S. Maranghi, L. Vesce, A. Sinicropi, A. Di Carlo, and R. Basosi, "Prospective Life Cycle Assessment of Third-Generation Photovoltaics at the Pre-Industrial Scale: A Long-Term Scenario Approach," *Renewable and Sustainable Energy Reviews* 121 (2020): 109703.

111. M. Salibi, F. Schönberger, Q. Makolli, E. Bousi, S. Almajali, and L. Friedrich, "Energy Payback Time of Photovoltaic Electricity Generated by Passivated Emitter and Rear Cell (PERC) Solar Modules: A Novel Methodology Proposal," in *Proceedings of the 38th European Photovoltaic Solar Energy Conference and Exhibition* (EU PVSEC, Lisbon, Portugal, 2021): 677-682.

112. J. Bastos, F. Monforti-Ferrario, and G. Melica, GHG Emission Factors for Electricity Consumption (European Commission, 2024), JRC136340.

113. A. Maalouf, T. Okoroafor, Z. Jehl, V. Babu, and S. Resalati, "A Comprehensive Review on Life Cycle Assessment of Commercial and Emerging Thin-Film Solar Cell Systems," *Renewable and Sustainable Energy Reviews* 186 (2023): 113652.

114. S. He, L. Qiu, L. K. Ono, and Y. Qi, "How Far Are We from Attaining 10-Year Lifetime for Metal Halide Perovskite Solar Cells?," *Materials Science and Engineering: R: Reports* 140 (2020): 100545.

115. X. Tian, B. Roose, S. D. Stranks, and F. You, "Periodic Module Rejuvenation Provides Early Market Entry for Circular All-Perovskite Tandem Photovoltaic Technologies," *Energy & Environmental Science* 16 (2023): 5551–5567.

116. R. Frischknecht, P. Stolz, G. Heath, M. Raugei, P. Sinha, and M. Wild-Scholten, Methodology Guidelines on Life Cycle Assessment of Photovoltaic Electricity, IEA PVPS Task 12, Report T12-18:2020 (International Energy Agency, 2020), https://iea-pvps.org/.